Journal of Alloys and Compounds 480 (2009) 454–461

Contents lists available at ScienceDirect

Journal of Alloys and Compounds

journal homepage: www.elsevier.com/locate/jallcom

Isothermal oxidation behavior of electrospark deposited MCrAlX-type coatings on a Ni-based superalloy

Yu-jiang Xie*, Mao-cai Wang

State Key Laboratory for Corrosion and Protection, Institute of Metal Research, Chinese Academy of Sciences, 62 Wencui Road, Shenyang 110016, PR China

ARTICLE INFO

Article history:
Received 24 October 2008
Received in revised form 18 January 2009
Accepted 22 January 2009
Available online 6 February 2009

Keywords:
Oxidation behavior
MCrAlX
Electrospark deposition
Repair

ABSTRACT

A MCrAlX-type coating has been prepared by electrospark deposition (ESD) and its isothermal oxidation behavior studied. The results indicate that deposition rate and surface roughness of the coatings increase with increasing spark pulse energy. A splattered porous morphology was observed in the surface layer, and underneath this, a uniform superfine columnar γ phase structure with a column width of about 0.6 μm. When exposed at 1000 °C, θ-Al_2O_3 formed rapidly in the early oxidation stage. After 100 h oxidation, a large amount of θ-Al_2O_3 was still present, and a dense and adherent, thin α-Al_2O_3 scale had formed beneath it.

1. Introduction

In recent years, cost effective repair and refurbishment of gas turbine blades has increasingly become an industrial practice because of economic considerations. For turbine blades operating in severe service conditions, in addition to the deterioration of the actual blade materials, the coatings will also gradually degrade with increasing service time, but not evenly due to extremely high surface temperatures at local areas of the component surface. This means that the coatings are prone to fail at these "hot points" while remaining acceptable elsewhere. In addition, there is a necessity to re-apply protective coating on the weld repair zone when turbine blades suffering from premature failure such as tip rubbing and tip cracking are considered for repair welding. In one sense, re-coating constitutes a critical step in the repair procedure of turbine blades. Usually, the whole coating on the blade surface is stripped and then replaced, which limits the number of permissable blade repairs to 2 or 3 because of blade wall thinning. Therefore, it is highly desirable that a cost effective method be developed to deposit protective coating in specific regions in a convenient way.

MCrAlX-type coatings are amongst the most important protective coating materials applied to counteract hot corrosion and high temperature oxidation. They are generally deposited by conventional thermal spraying methods such as vacuum or low pressure plasma spraying (VPS or LPPS) or high velocity oxygen fuel (HVOF). However, the density and homogeneity of the coatings and the bond strength between coating and substrate obtained by these techniques remain to be further improved [1], and moreover, a diffusion heat-treatment is generally required. In contrast, it is possible with electrospark deposition (ESD) to produce coatings with a high density and good homogeneity [2]. Moreover, parts can be recoated in the final heat-treated condition without subsequent heat-treatment since this process uses short-duration high current pulses to weld the coating material on the substrate at or near ambient temperature, thus preventing thermal distortion or metallurgical change in the thermally sensitive substrate [3]. In addition, electrospark deposition is also a relatively simple, highly efficient and inexpensive method for surface treatment. It has originally been used to generate wear- and/or corrosion-resistant coatings [4–6], but recently it has been used to prepare high temperature oxidation-resistant coatings such as oxide dispersion strengthened (ODS) alloy coating [7,8], $TiAl_3$ coatings [9] and FeCrAl coating [10], and their oxidation behavior has been extensively studied. Some work has been carried out on the preparation of MCrAlX-type coatings by electrospark deposition [2,11], but this concentrated mainly on their formation mechanism and their microstructural characteristics, and investigations of their oxidation behavior have been limited.

In the present work, thick MCrAlX coatings have been deposited on the surface of a Ni-base superalloy by ESD, and their metallurgical properties and isothermal oxidation behavior have been studied.

2. Experimental

A Ni-base superalloy, IN-792, with the composition of Ni–11.5Cr–8.5Co–3.3Al–3.35Ti–1.85Mo–3.7W–3.9Ta–0.05Zr wt.%, was cut into specimens with dimensions of 10 mm × 15 mm × 2 mm as the substrate material.

* Corresponding author. Tel.: +86 24 23915863; fax: +86 24 23890049.
E-mail address: yjxie@imr.ac.cn (Y.-j. Xie).

0925-8388/$ – see front matter © 2009 Elsevier B.V. All rights reserved.
doi:10.1016/j.jallcom.2009.01.100

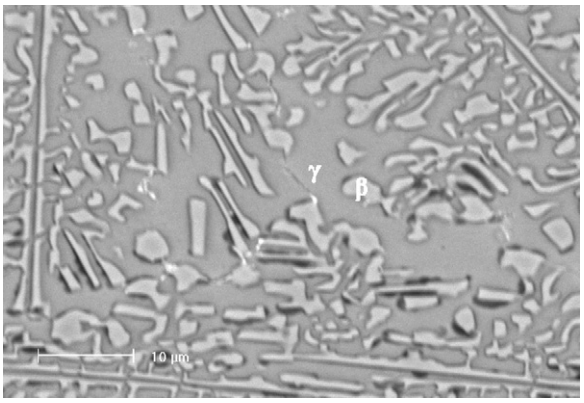

Fig. 1. Microstructure of the NiCoCrAlYTa electrode material.

The surface was ground to 600 grit SiC, cleaned ultrasonically in alcohol, and then blown dry. A MCrAlX-type alloy rod, made from a powder with a composition of Ni–23Co–20Cr–8Al–4Ta–0.6Y by laser direct forming was used as the electrode material. The size of the electrode was Ø3.5 mm × 50 mm. The electrode exhibited γ/β structure with a dispersion of β phase (Ni, Co)Al in the (Ni, Co, Cr)-rich γ phase solid solution matrix as shown in Fig. 1.

A 3H-ES-6 ESD processing machine, which has been described previously [12], was employed to deposit the coating. The processing parameters can be adjusted: capacitance (up to 420 μF), voltage (up to 100 V) and frequency (up to 2000 Hz). The product of the capacitance (C) and the voltage (V) is usually calculated as the pulse energy (E), namely, $E = 1/2CV^2$. The experiments were conducted at a fixed capacitance of 420 μF, a fixed frequency of 300 Hz, and varied voltages of 40, 60, 80 and 100 V, respectively. The deposition was carried out using a hand-held gun at room temperature with argon protection. The NiCoCrAlYTa coating was deposited on a plane of 10 mm × 15 mm of the specimen. The surface area can be effectively covered for one time in about 30 s traveling time. The deposition rate of the coatings was evaluated by measuring the mass change every 2 min of a process lasting a total time of 10 min. Surface roughness of the coatings was measured by using a surface profilometer with a precision of 0.01 μm.

Isothermal oxidation tests were carried out in ambient air in a muffle furnace at 1000 °C. The specimens were put in alumina crucibles, oxidized at elevated temperature and then cooled to room temperature at regular intervals for mass measurement. The sensitivity of the electronic balance used was 0.1 mg.

The phase compositions of the deposited coatings before and after oxidation were identified by means of X-ray diffractometry (XRD). The morphologies and chemical compositions of the coatings and the oxide scale were observed and determined by scanning electron microscopy (SEM) equipped with an energy dispersive spectrometer (EDS).

3. Results

3.1. The preparation of the coatings

Fig. 2 shows curves of mass gain of NiCoCrAlYTa coating vs. deposition time at different spark pulse energies. It can be seen that the mass gain of the coatings was in direct proportion to deposition time, and the deposition rate increased from 3.3 to 11.3 mg/min when the pulse energy increased from 0.336 to 2.1 J. Table 1 lists the surface roughness of a coating produced at pulse energies of 0.336, 0.756, 1.334 and 2.1 J, respectively. It can be seen that surface roughness increases with increasing pulse energy at a fixed frequency of 300 Hz. A rough surface (Ra 12.345) could be obtained at a high pulse energy (2.1 J) and a relatively smooth surface (Ra 7.54 μm) at a relatively low pulse energy (0.336 J). Moreover, the surface roughness was lower (Ra 5.62 μm) when the frequency was raised to 2000 Hz with a pulse energy of 0.336 J.

Table 1
Surface roughness of NiCoCrAlYTa coating under different pulse energies.

Surface roughness (μm)	Pulse energy (J)
7.540	0.336
9.401	0.756
11.612	1.334
12.345	2.1

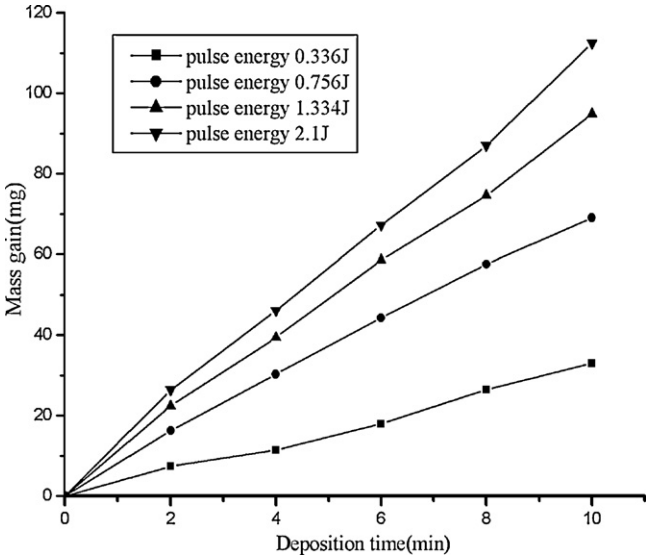

Fig. 2. Mass gain of NiCoCrAlYTa coating vs. deposition time under different pulse energies.

Fig. 3 shows the surface morphology of electrospark deposited NiCoCrAlYTa coating. It could be clearly seen that the surface of the coating was not smooth and continuous, exhibiting apparently a splattered appearance and the last splat superimposed on the previous layer (Fig. 3a). A closer examination using scanning electron

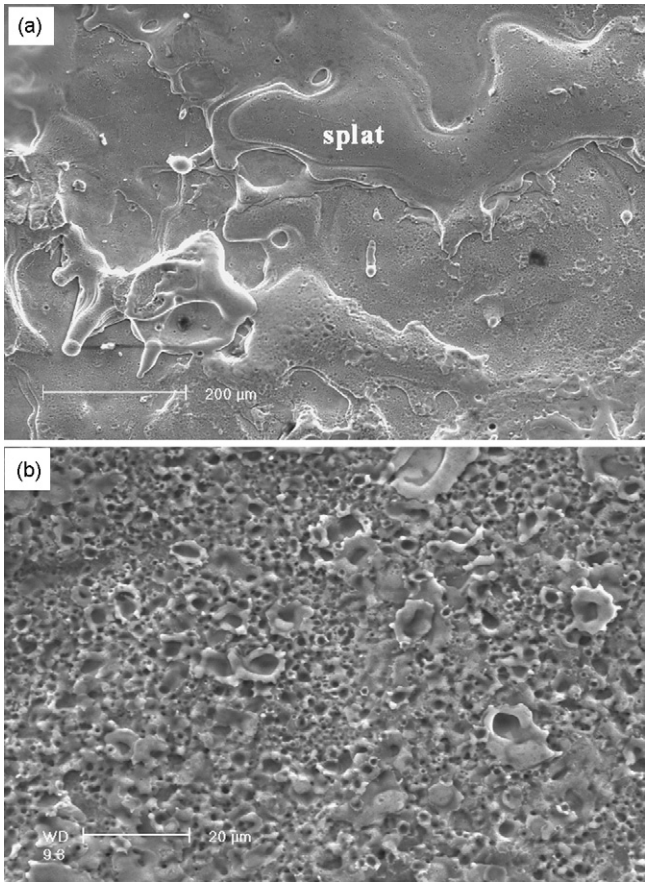

Fig. 3. Surface morpholoy of NiCoCrAlYTa coating: (a) low magnification; (b) high magnification.

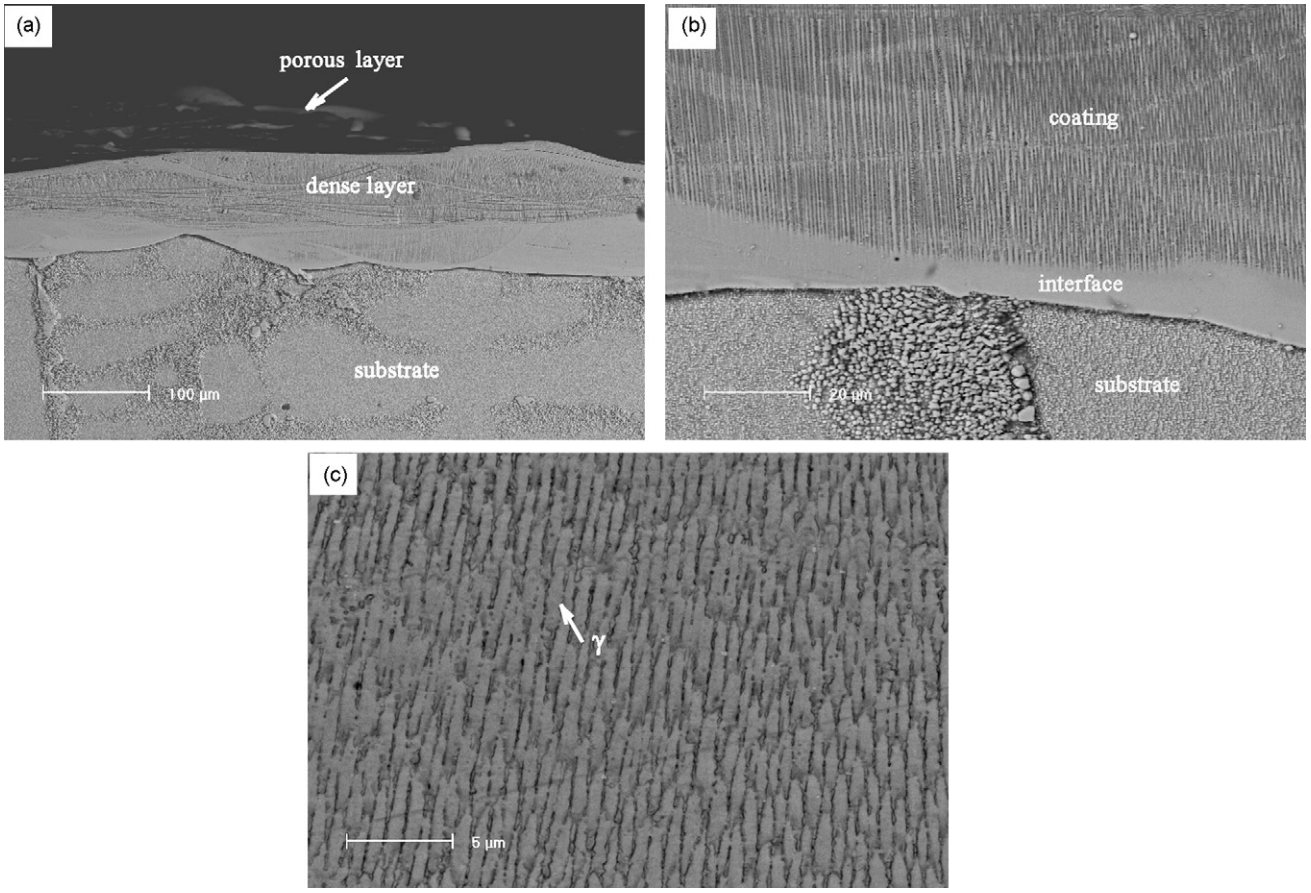

Fig. 4. Cross-sectional morphologies of NiCoCrAlYTa coating: (a) low magnification image showing the whole coating; (b) interface between coating and substrate; (c) microstructure of the coating.

microscopy confirmed that there were numerous small particles stuck in the surface (Fig. 3b).

Fig. 4 shows the cross-sectional morphology of electrospark deposited NiCoCrAlYTa coating. The coating was composed of two layers, a porous outer layer and a fully dense inner layer (Fig. 4a). EDS analysis results showed that the coating had an average composition of (44.62Ni, 19.19Cr, 22.05Co, 8.25Al, 5.89Ta wt.%), close to the original composition of the coating alloy. Between the substrate and the coating, there is a clearly visible fusion layer (Fig. 4b), indicating that a continuous, adherent metallurgical bond had been obtained. The microstructure of the coating consisted of uniform short superfine columnar crystals with a column width of about 0.6 μm (Fig. 4c), which was totally different from the microstructure of the electrode used for the ESD processing (Fig. 1). XRD analysis results show that the coating consisted of only the single γ phase (Fig. 5), which indicates that the ESD process can be beneficial to the formation of a homogenous coating when the less homogenous NiCoCrAlYTTa electrode with a dual phase γ/β structure is used.

3.2. Isothermal oxidation results

Fig. 6 shows oxidation kinetics of NiCoCrAlYTa-coated and bare IN-792 specimen at 1000 °C for 100 h. For comparison, the oxidation kinetics of the NiCoCrAlYTa electrode alloy are also plotted in Fig. 6. The oxidation kinetics of the uncoated IN-792 specimens followed an apparently parabolic rate law, while the behavior of the coated specimens was different: the mass gain increased rapidly during the first 5 h, then levelled off. The oxidation behavior of the specimen with the NiCoCrAlYTa coating was far superior to that of the uncoated specimen, and after 100 h its weight gain was only 1/6 of that of the latter. The results indicated that the oxidation resistance of IN-792 alloy was obviously improved by covering NiCoCrAlYTa coatings. Compared with NiCoCrAlYTa electrode alloy, the ESD NiCoCrAlYTa coating had a lower oxidation rate except in the first 5 h, indicating the microstructural homogeneity and refinement had a beneficial effect on the oxidation resistance.

X-ray analysis of the oxide scale of the NiCoCrAlYTa coating formed after 2 h and 100 h is presented in Fig. 7. θ-Al_2O_3 peaks

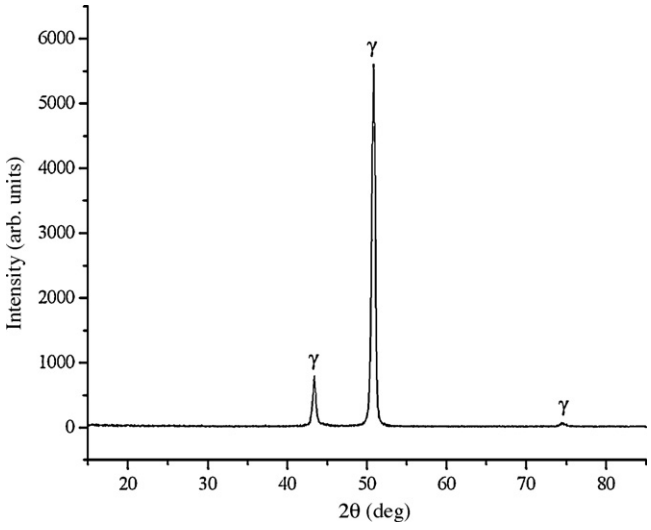

Fig. 5. X-ray diffraction patterns of the coating.

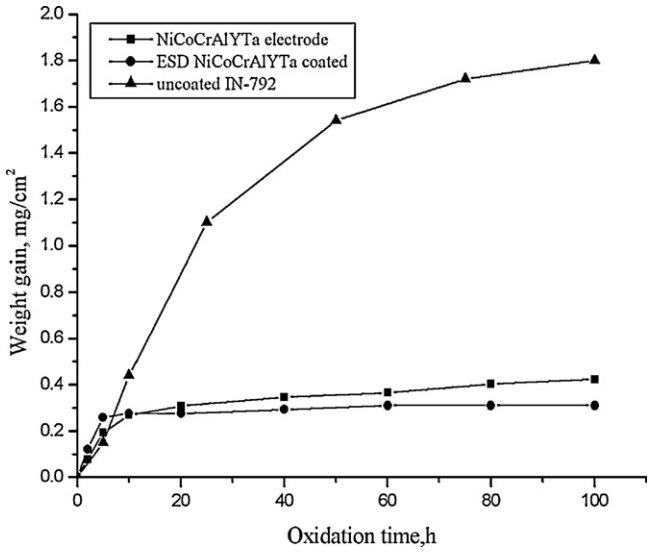

Fig. 6. Oxidation kinetics curves of NiCoCrAlYTa electrode specimens, ESD NiCoCrAlYTa coated and uncoated IN-792 specimens at 1000 °C for 100 h.

were present after 2 h oxidation; after 100 h, they were weaker, and α-Al_2O_3, peaks had appeared.

Fig. 8 shows the surface morphologies of oxide scale formed at 1000 °C in air after 2 h. The surface was mainly covered by needle-like oxide corresponding to θ-Al_2O_3 [13]. Fig. 9 shows the surface morphology of the coating that had been oxidized at 1000 °C for 100 h. At low magnification, three typical areas with different color contrast can be found in Fig. 9a, a white area with scattered white spots (area 1), a dark area (area 2) and a light area (area 3). At higher magnification, it was found that the white spots were agglomerations of oxide grains on the surface of the scale (Fig. 9b, area 1). EDS analysis of these white spots gave strong Cr, Ni, Co and O peaks and small Al peaks (Fig. 10a), which suggests that the white oxide could be the (Ni, Co) (Cr, Al)$_2O_4$ spinel phase. In the dark area (Fig. 9c, area 2), the oxides were porous and coarsely needle-like. EDS analysis detected the presence of Cr, Al and O, with Al and O the most prominent (Fig. 10b). The needle-like morphology suggests that the oxide was θ-Al_2O_3. In the light area (Fig. 9d, area 3), besides a few scattered coarse needles, most of the oxide was fine-grained and very compact. EDX analysis showed that the oxides were rich in Al and O (Fig. 10c). From the XRD analysis results, this is believed to be α-Al_2O_3. α-Al_2O_3, usually with an equiaxed crystal structure, has

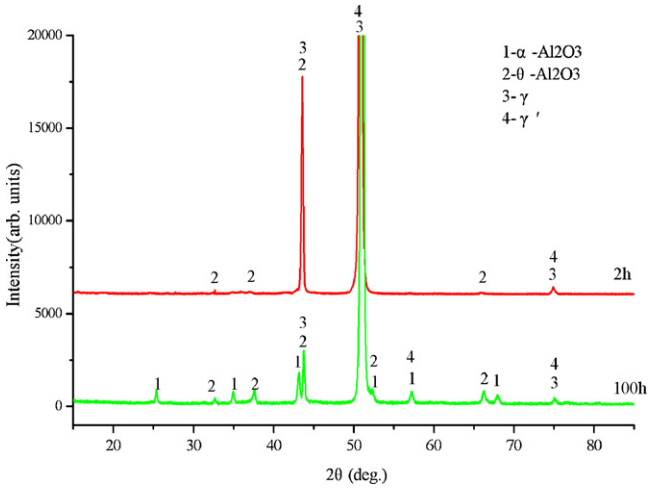

Fig. 7. X-ray diffraction patterns of NiCoCrAlYTa coating oxidized for different times.

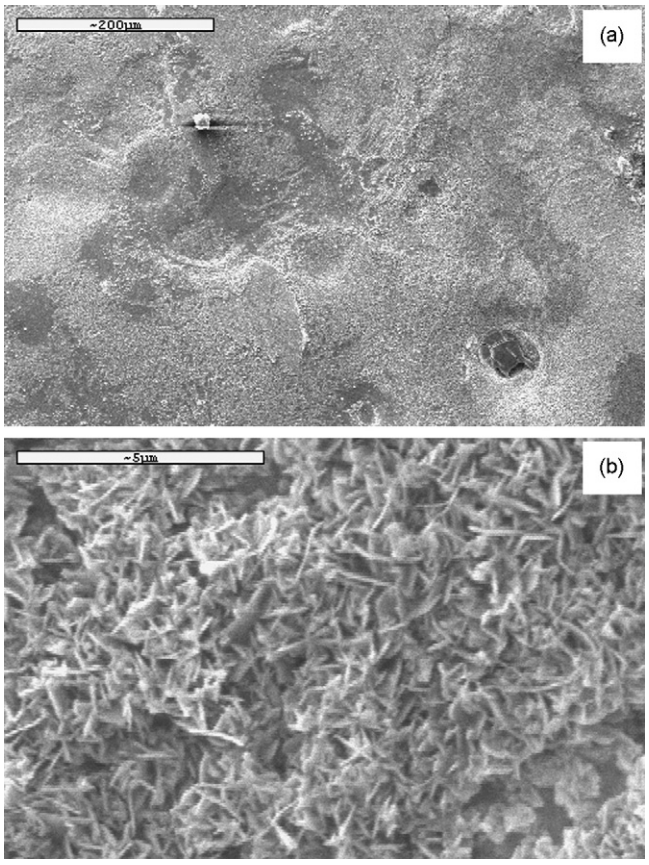

Fig. 8. Surface morphologies of oxide scale formed at 1000 °C in air after 2 h: (a) low magnification; (b) high magnification.

previously been found to form beneath needle-like θ-Al_2O_3 after 100 h oxidation at 1000 °C [14].

Fig. 11 presents cross-sectional morphologies of NiCoCrAlYTa coating after oxidation at 1000 °C for 100 h. From Fig. 11a, it can be clearly seen that there was an outer degraded layer about 20 μm thick below the Al-rich oxide, beneath that there was the unaffected coating about 75 μm thick and then an inter-diffusion zone of about 10 μm formed between the coating and the substrate. In the unaffected bulk of the coating, the columnar structure had completely disappeared, and instead a large number of black phases and white spot phases were dispersed in the light-phase matrix (Fig. 11b). EDS was used to determine the phase compositions and the results were shown in Table 2. The light phase contained 4.24 wt.% Al, the black phase contained 16.96 wt.% Al, whereas the white spot phase contained 7.09 wt.% Al and 17.76 wt.% Ta with an atom percent ratio of Al content and Ni content close to 1:3. On the basis of these results, the NiCoCrAlYTa coating is believed to consist of three metallic phases: a matrix of γ-(Co, Ni)Cr, with dispersed β-NiAl and γ'-Ni_3(Al, Ta), which is in good agreement with the structure of the annealed heat-treated NiCoCrAlYTa HVOF coatings[14]. The outer part of the degraded layer was composed only of γ phase, and had been depleted completely of the γ' and β phases. Beneath this it consisted of the γ' and γ phases, and had been depleted completely

Table 2
EDS analysis results of different phases in Fig. 11b (wt.%).

	Al	Ta	Cr	Co	Ni
White spot phase	7.09	17.76	12.63	17.00	45.52
Black phase	16.96	4.31	12.99	17.09	48.65
Light phase	4.61	5.94	23.38	27.12	38.95

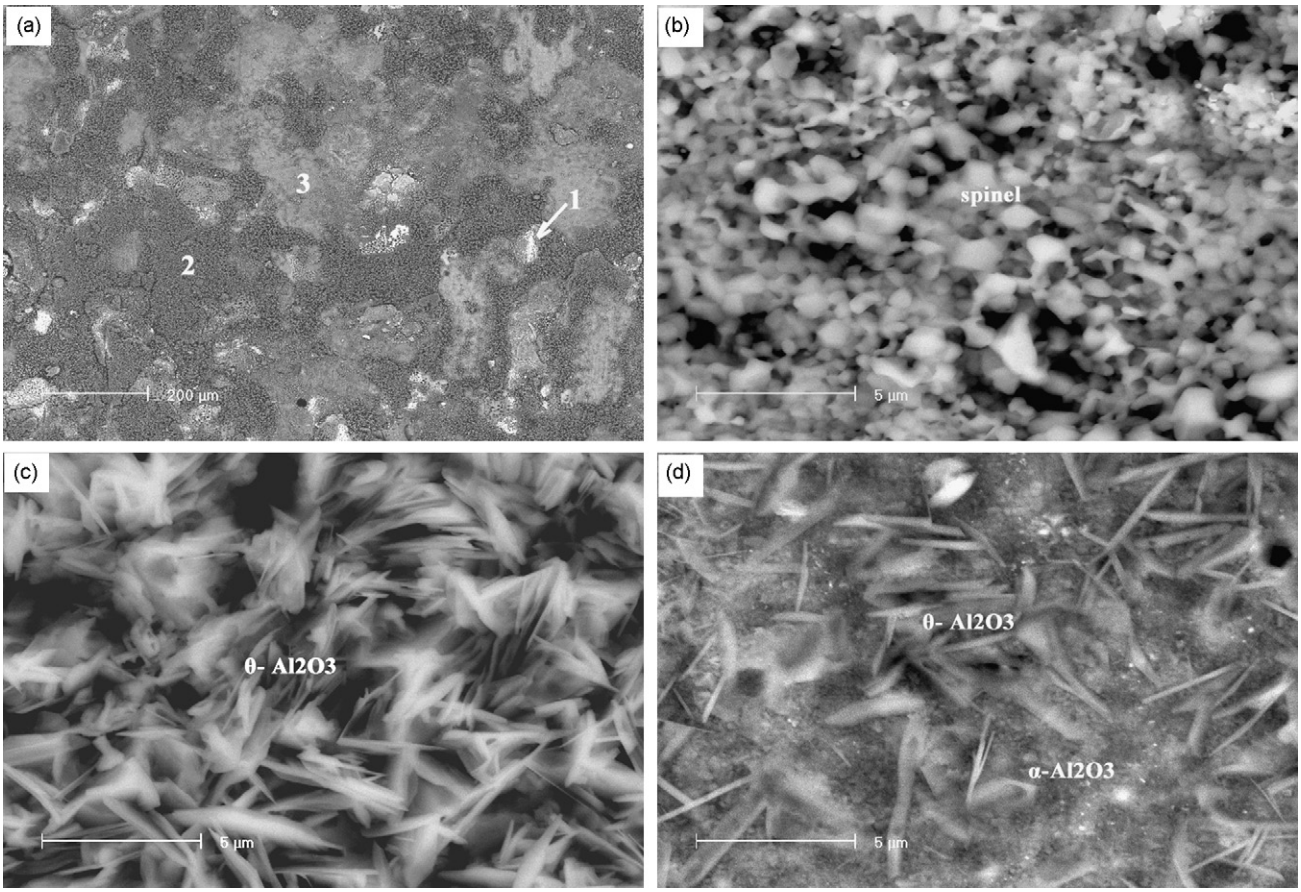

Fig. 9. Surface morphologies of oxide scale formed at 1000 °C in air after 100 h : (a) low magnification view; (b–d) higher magnification images of area 1, area 2 and area 3, respectively.

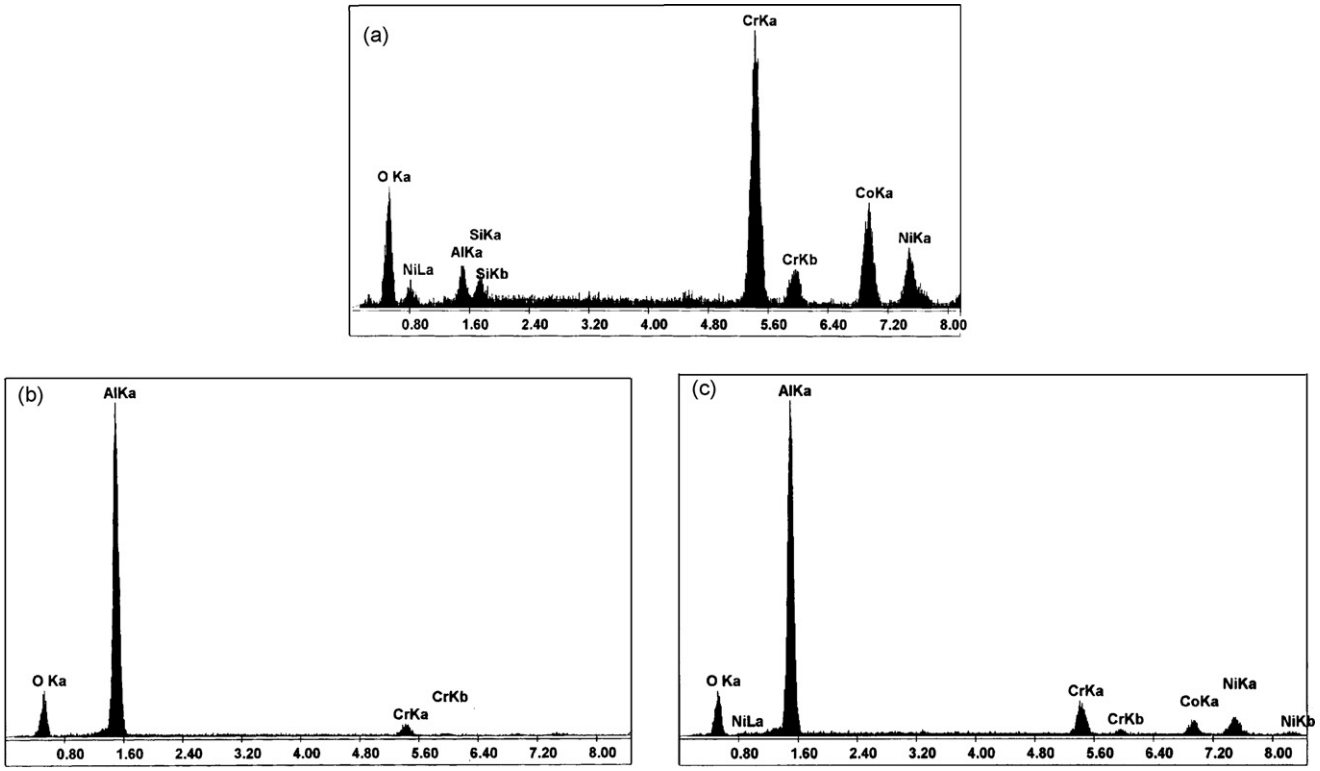

Fig. 10. (a–c) EDS analysis results of area 1, area 2 and area 3, respectively.

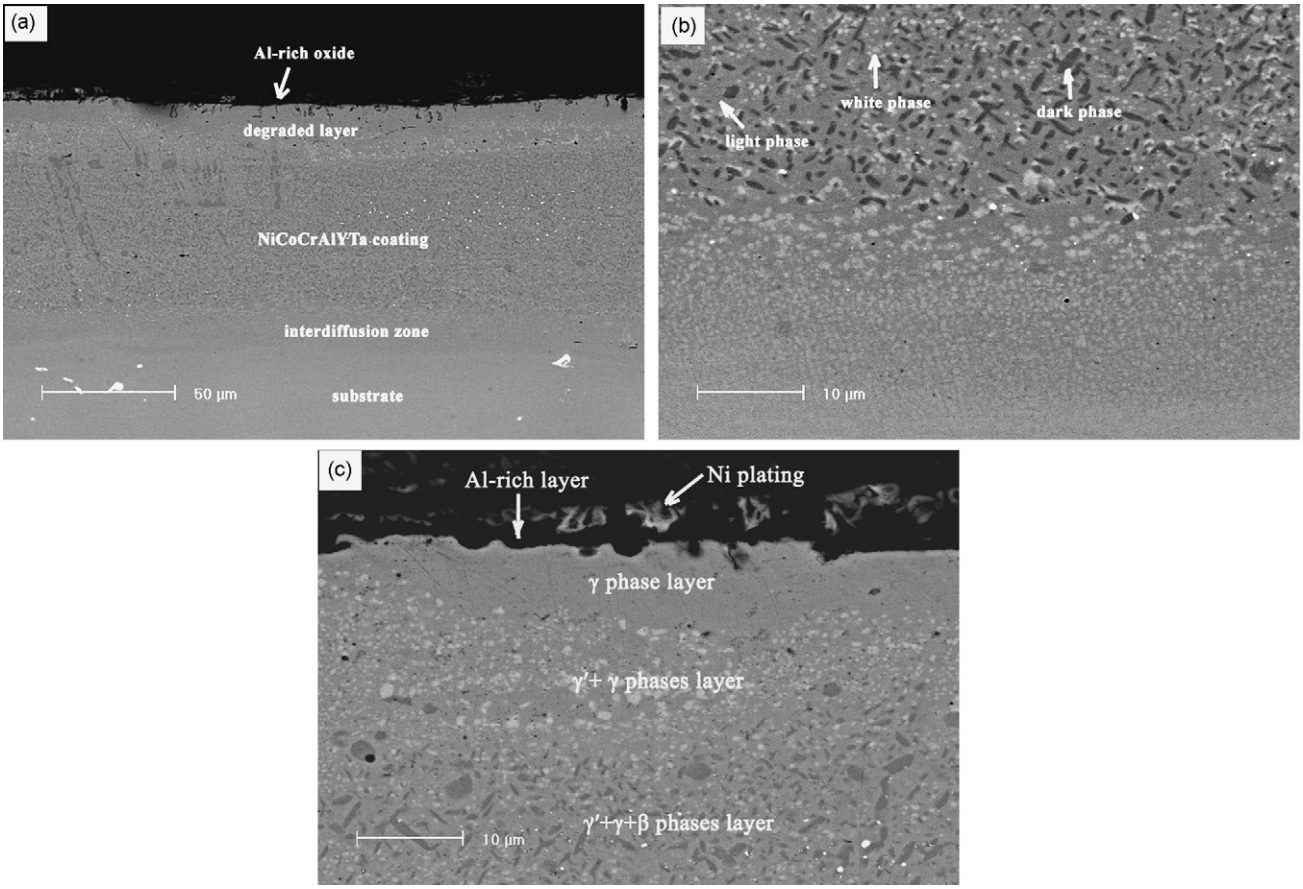

Fig. 11. Cross-sectional morphologies of oxide scale formed at 1000 °C in air after 100 h: (a) low magnification view; (b) interface between the substrate and coating; (c) oxidized region.

of the β phases. Al consumption during the oxidation is believed to have led to the transformation of β to γ′ to γ.

Fig. 12 displays the micrograph and elemental X-ray maps of a cross-section of the NiCoCrAlYTa coating obtained after oxidation in air at 1000 °C for 100 h. The maps of Ni, Co, Cr, Al and Ta, confirmed that the γ phase contained mainly Ni, Co and Cr, and the γ′ phase contained mainly Ni, Al and Ta. From the maps of Al, O, Co, Cr and protective Ni plating, it can be seen that the oxide scale consisted of two layers, a thick outer layer thought to be a complex oxide including θ-Al_2O_3 and minor spinel, and an adherent thin inner layer assumed to be α-Al_2O_3. In addition, from image mapping of Y, it seems that there is a preferential enrichment of Y immediately below the oxide/coating interface, resulting in a depleted layer beneath that.

4. Discussion

The ESD process basically utilizes short-duration electrical pulses, discharges at controlled energy levels, to create a metallurgically bonded surface modification. Pulse energy and pulse frequency can be adjusted to achieve various deposition conditions. In the early ESD equipment, the electrode is mechanically vibrated to connect and break the circuits, generating sparks. The spark frequency is thus controlled by the vibration frequency of the electrode, normally less than 100 Hz. With that technique, the deposition rate and surface roughness of a coating were closely related to the electrical parameters. The deposition rate increased with increasing vibration frequency and spark pulse energy, but high spark pulse energy will lead to poor surface quality. It has been reported [11] that MCrAlY coatings of thickness up to 500 μm were obtained using the conventional ESD installation under the following conditions: vibration frequency 100 Hz, pulse energy 7.5 J, which would readily result in a rough surface. In the present study, the use of the high power IGBT electric switches and a spark frequency up to 2000 Hz independent of the rotation of the electrode provides a high flexibility. A high pulse energy with a low spark frequency can be used to obtain a thick coating in a short time while a low pulse energy with a high spark frequency are preferred for good surface quality of the coating.

Electrospark deposition is a micro-welding process and microwelds produced by spark discharge can metallurgically bond, even epitaxially grow to form a dense multi-layer coating [2]. High cooling rates inherent in this process can approach 10^5 to 10^6 K/s, as a result, microstructure coarsening and solute segregation will be suppressed, so that a good homogenization of the coating is likely to be achieved. According to the XRD/EDS results and the cross-sectional SEM micrographs, the microstructure of electrospark deposited NiCoCrAlYTa coating is characterized by the retention of a homogeneous single γ phase structure with superfine columnar dendrites and a significantly higher concentration of key alloying elements (such as Al, Cr and Y), which is quite different from that of NiCoCrAlYTa coating with γ/β structure produced by conventional methods such as VPS and HVOF [15,16]. The microstructure of NiCoCrAlYTa VPS coating remains γ and β phases even after laser remelting [17]. This is a considerable advantage of the ESD process in obtaining a homogenous and refined coating. Microstructure refinement and homogeneity of MCrAlX coatings have been previously made by laser or electron beam treatment [18–20]. It has been found that the oxidation resistance of MCrAlX alloys was improved by these welding processes, a beneficial effect which is attributed

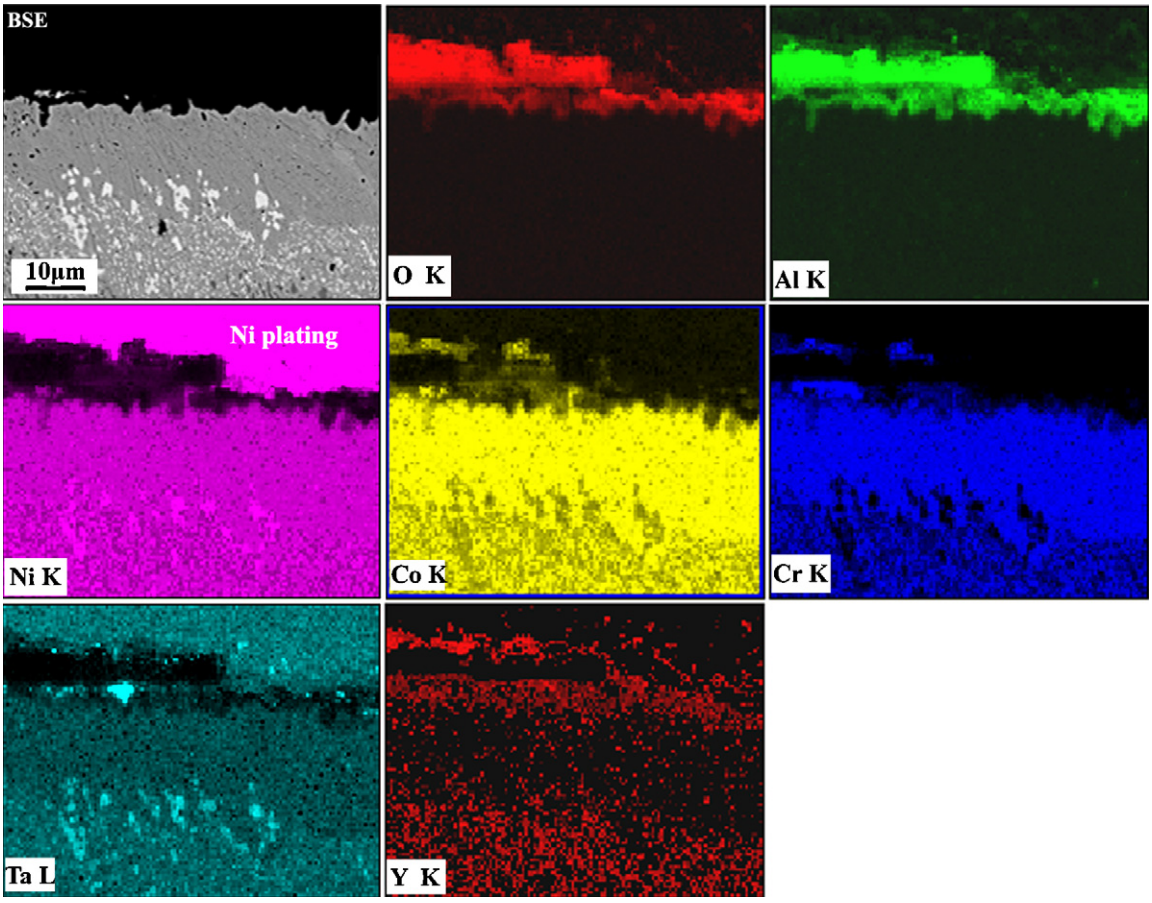

Fig. 12. Micrograph and elemental X-ray mappings of a cross-section of oxide scale formed at 1000 °C in air after 100 h.

to excellent bonding of the coating to the substrate and to the fact that the coating was fully dense.

Needle-like oxides had formed on the coatings after 2 h oxidation tests as shown in Fig. 8(b). It has been shown that the needle-like oxide is θ-Al_2O_3 which is a metastable phase and will transform to the thermodynamically stable α-Al_2O_3 phase. It has been found that the coatings with a higher Al content had a stronger tendency to form θ-Al_2O_3 than the coatings with a lower Al content [21]. θ-Al_2O_3 scale grows at a higher rate than α-Al_2O_3 scale. It was believed that the fast diffusion of Al in the initial oxidation stage promoted the formation of the fast-growing θ-Al_2O_3. The formation of fast-growing θ-Al_2O_3 explains why the coatings showed higher oxidation mass gains in the early oxidation stage than the uncoated specimens. After some time, θ-Al_2O_3 grains transformed to α-Al_2O_3. The oxidation rate will then slow down because α-Al_2O_3 scale has a slow growth rate. The transformation from θ to α phase explains why the oxidation mass gain curve of the coating levelled off after some time of oxidation, as shown in Fig. 6.

On the other hand, a major disadvantage with electrospark coating that has still not been effectively controlled may be the rough and spattered surface resulting from the splat of tiny droplets during the deposition. These droplets may only be a few micrometers in diameter but they are sufficiently large to form scattered particles on the surface when they cool and solidify. As was observed in Fig. 3b, the surface layer of electrospark deposited coating was not fully dense, scattered with a great number of porous spattering particles. When exposed to at 1000 °C, the surface layer would first oxidize, but a continuous Al_2O_3 layer was not established because of separation of those spattering particles, and instead a complex outer oxide scale including θ-Al_2O_3 and spinel was formed. With the diffusion of oxidation, the fully dense inner layer began to oxidize, β and γ′ degraded to form γ due to outward diffusion of Al, and ultimately a dense and complete α-Al_2O_3 thin scale was formed.

5. Conclusion

Electrospark deposition technique can be used to prepare NiCoCrAlYTa coatings. The deposition rate and surface roughness of the coatings increased with increasing spark pulse energy. The ESD coating had a porous outer layer, but beneath this it had a fully dense metal layer, which was metallurgically bonded to the substrate. It had a uniform superfine columnar γ phase structure with a column width of about 0.6 μm.

When exposed at 1000 °C for 100 h, the rough and porous surface layer of the NiCoCrAlYTa coating rapidly formed a complex oxide scale including θ-Al_2O_3, spinel, but beneath that layer, a dense and adherent α-Al_2O_3 thin scale formed.

The good oxidation resistance of ESD NiCoCrAlYTa coating is attributed to the fact that electrospark rapid solidification processes results in a homogenous and dense coating with the remarkably higher concentration of Al in the microstructure.

Acknowledgements

The work is supported by the National Natural Science Foundation of China (Grant No. 50671116) and the Knowledge Innovation Program of the Chinese Academy of Sciences.

References

[1] Y.P. Zhang, Z.R. Zhou, J.M. Cheng, Y.L.G. He, H. Ma, Surf. Coat. Technol. 79 (1996) 131–134.

[2] Y.J. Xie, M.C. Wang, Surf. Coat. Technol. 201 (2006) 3564–3570.
[3] R.N. Johnson, Society of Vacuum Coaters 45th Annual Technical Conference, Lake Buena Vista, FL, April 13–18, 2002, pp. 87–92.
[4] R.J. Wang, Y.Y. Qian, J. Liu, Appl. Surf. Sci. 240 (2005) 42–47.
[5] S. Frangini, A. Masci, A. Di Bartolomeo, Surf. Coat. Technol. 149 (2002) 279–286.
[6] J. Liang, W. Gao, Z. Li, et al., Mater. Lett. 58 (2004) 3280–3284.
[7] Y. He, H. Pang, H. Qi, D. Wang, Z. Li, W. Gao, Mater. Sci. Eng. A 334 (2002) 179–186.
[8] W. Gao, Z.Y. Liu, Z. Li, Adv. Mater. 13 (2001) 1001–1004.
[9] Z.W. Li, W. Gao, Y.D. He, Scr. Mater. 45 (2001) 1099–1105.
[10] W. Gao, Z. Li, Y. He, Mater. Sci. Forum 369–372 (2001) 579–586.
[11] A.V. Paustovskii, R.A. Alfintseva, T.V. Kurinnaya, V.V. Pogorelaya, S.N. Kirilenko, Powder Metall. Met. Ceram. 43 (5–6) (2004) 251–257.
[12] Y.J. Xie, M.C. Wang, Surf. Coat. Technol. 201 (2006) 691–698.
[13] J.L. Smialek, J. Doychak, D.J. Gaydosh, Oxid. Met. 34 (1990) 259–266.
[14] C.T. Liu, X.F. Sun, H.R. Guan, Z.Q. Hu, Surf. Coat. Technol. 194 (2005) 111–118.
[15] S. Pahlavanyali, A. Sabour, M. Hirbod, Mater. Corros. 54 (2003) 687–693.
[16] S. Li, C. Langladc, S. Faycullc, D. Treheux, Surf. Coat. Technol. 100–101 (1998) 7–11.
[17] R. Streiff, M. Pons, P. Mazars, Surf. Coat. Technol. 32 (1987) 85–95.
[18] H. Iwamoto, T. Sumikawa, K. Nishida, T. Asano, M. Nishida, T. Araki, Mater. Sci. Eng. A 241 (1998) 251–258.
[19] C.R. Ribaudo, J. Mazumder, D.W. Hetzner, Metall. Trans. B 23B (1992) 513–522.
[20] U. Dragos, M. Gabriela, B. Waltraut, C. Ioan, Solid State Sci. 7 (2005) 459–464.
[21] Z. Liu, W. Gao, G. Hao, Scr. Mater. 38 (1998) 1057–1063.